PAPER

Tunable low-frequency torsional-wave band gaps in a meta-shaft

IOP Publishing Journal of Physics D: Applied Physics
J. Phys. D: Appl. Phys. **52** (2019) 055104 (13pp) https://doi.org/10.1088/1361-6463/aaf039

Tunable low-frequency torsional-wave band gaps in a meta-shaft

Kai Wang[1,2], Jiaxi Zhou[1,2,4], Daolin Xu[1,2] and Huajiang Ouyang[3]

[1] State Key Laboratory of Advanced Design and Manufacturing for Vehicle Body, Hunan University, Changsha 410082, People's Republic of China
[2] College of Mechanical and Vehicle Engineering, Hunan University, Changsha 410082, People's Republic of China
[3] School of Engineering, University of Liverpool, Liverpool L69 3GH, United Kingdom

E-mail: jxizhou@hnu.edu.cn

Received 14 August 2018, revised 5 November 2018
Accepted for publication 12 November 2018
Published 26 November 2018

Abstract

The location of a locally resonant band gap is related to the resonant frequency of the local resonator, and thus one could obtain a band gap in a very low-frequency region by designing a resonator with an ultra-low resonant frequency. In this paper, a novel torsional resonator is proposed by introducing a negative stiffness mechanism composed of five pairs of cams and rollers to partially neutralize the positive stiffness of a rubber ring. By attaching this resonator onto an elastic shaft, a meta-shaft structure for attenuating low-frequency torsional wave is devised. The static analysis for the local resonator and the dynamic analysis for the meta-shaft are conducted. The band structure is revealed by the transfer matrix method, which are validated by numerical simulations with the assistance of the Galerkin method. The theoretical results show that the location of the band gap can be effectively shifted from the high frequency region to a lower one by tuning down the net stiffness of the resonator. In addition, the effects of structural parameters on the band gap and torsional wave attenuation are also evaluated, which indicate that a thick rubber ring, a large number of unit cells and a small-amplitude excitation are beneficial to open a broad and deep band gap at low frequencies. This could be a potential solution to the challenge of low-frequency torsional wave attenuation.

Keywords: meta-shaft, low-frequency band gaps, torsional wave attenuation, negative stiffness mechanism, nonlinear local resonator

(Some figures may appear in colour only in the online journal)

1. Introduction

Phononic crystal, an artificial periodic material, has the ability to create a frequency band useful for applications such as acoustic and elastic waveguides [1–3], wave filters [4, 5], vibration control [6–8], acoustic cloaks [9, 10], acoustic topological insulators [11, 12] and energy harvesting devices [13, 14]. Generally, there are two types of mechanisms, namely, the Bragg scattering (BS) mechanism and local resonance mechanism for opening a band gap. Actually, the location of the band gap created by BS mechanism is related to the lattice constant which should be equal to the wave length, while the central frequency of the local resonant band gap is related to the resonant frequency of the resonator [15, 16]. Therefore, the local resonance mechanism can open a band gap in a lower frequency region, compared with the Bragg scattering mechanism.

In the past two decades, numerous investigations have been carried out to create low-frequency band gaps by employing locally resonant structures. For the sake of brevity, a short review of these closely related to the topic of this paper is given as follows. Lazaron and Jensen [17] studied a 1D chain with a series of nonlinear resonators, and both the linear and nonlinear dispersion relations have been derived. Xiao *et al* [18–20] attached mass-spring resonators and beam-like resonators on a beam respectively to form periodic structures, and studied their band structures and flexural wave propagation in such

[4] Author to whom any correspondence should be addressed.

locally resonant beams. Wang *et al* [21] proposed a continuum beam resonator. Wang *et al* [6, 22] created multi-flexural band gaps in a periodic beam by lateral resonators. Xiao *et al* [23] expand the application of the spring-mass resonators by attaching it on a thin plate and studying the bending wave propagation characteristics in different directions. Zhou *et al* [24] also proposed a two-dimensional (2D) periodic structure with multilayered locally resonators. Utilizing inclined ligament, Bigoni *et al* [25] proposed a inertial locally resonant and designed an elastic metamaterial based on it to create tunable low-frequency band gaps. Bacigalupo and Gambarotta [26] also proposed a beam-lattices metamaterial with inertial resonators by elastic elements. Liu *et al* [27] designed a 3D locally resonant elastomer composed of a high-density solid core and soft elastic materials.

In order to widen a band gap, Frandsen *et al* [28] and Li and Li [29] proposed an inertial-amplification mechanism and embedded it into the resonator to broaden the band gap. Liu and Reina [30] proposed a hierarchical structure to obtain an ultra-broad band gap. Wang and Wang [31] attached force-moment resonators on a beam to do it. Both the theoretical and experimental results in the above works indicate that the local resonators can form a band gap around its resonant frequency, which provides a potential application for attenuating the elastic wave at a targeted frequency by designing a unique local resonator.

However, most of those works focused on the band gaps for longitudinal waves and flexural waves [15], and the studies on attenuating torsional waves by locally resonant shafts are rare. Generally, it is a common method to mitigate torsional vibration by torsional vibration isolators [32–34], but the locally resonant shaft could provide an way to absorb torsional vibration. Yu *et al* [35] proposed a shaft with periodically attached local resonators to create a band gap, and thus to control torsional vibration in a targeted frequency region. Shu *et al* [36] used piezoelectric ceramic circular rings to construct a periodic shaft for opening a torsional wave band gap. Li *et al* [8] utilized double locally resonant effects to design a periodic shaft for controlling the propagation of the torsional wave.

In general, the previous works about the locally resonant mechanisms, including those used to attenuate bending waves, longitudinal waves and torsional waves, failed to create a band gap in very low-frequency region. Because the resonant frequency of the local resonator is related to its mass and stiffness, and it is difficult to design a resonator with ultra-large mass and ultra-low stiffness [37]. Fortunately, a negative-stiffness mechanism (NSM) could help to resolve this problem, due to its capability of counteracting the stiffness of the positive-stiffness element to construct a high-static-low-dynamic-stiffness (HSLDS) system [38–41]. In one previous work of the authors', an HSLDS local resonator was proposed by combining a positive-stiffness spring with an NSM. The stiffness of the spring was partially or totally neutralized by the NSM, so that the net stiffness of resonator can be tuned to desired low values [42, 43]. By attaching such resonators periodically, the locally resonant beam can open a band gap for attenuating flexural waves in a very low-frequency region. Moreover, the location of the band gap can be easily tuned by adjusting the parameters of the resonator; therefore, it can be used to control waves at a targeted low frequency.

The main contribution of this paper is to develop a torsional HSLDS resonator to attenuate very low-frequency torsional wave propagating in a shaft. The HSLDS resonator is composed of a rubber ring and five pairs of cam-roller-spring mechanisms. In this resonator, the negative stiffness is realized by the cam-roller-spring mechanism, which is utilized to partially or totally neutralize the positive stiffness provided by the rubber ring. Therefore, the net stiffness of the resonator can be tuned towards a desired low value to create a very low-frequency band gap for torsional waves in the shaft.

This paper is organized as follows: in section 2, both the physical and computational models of the local resonator and the meta-shaft are presented, and the static analysis of the resonator is conducted. The dispersion relations and band structures are obtained by using the transfer matrix method in section 3. In section 4, numerical simulations of the meta-shaft are carried out. The effects of the damping of the local resonator, the number of unit cells and the excitation amplitude on band structures and torsional wave attenuation are discussed. Finally, some conclusions are drawn in section 5.

2. Conceptual design and static analysis

Figures 1(a) and (b) show the physical models of a meta-shaft and an HSLDS resonator, respectively. The fundamental building block of this HSLDS resonator is a metal mass ring (7) connected to an epoxy shaft (6) by both a vulcanized rubber ring (with thickness l) (5) and an NSM composed of five pairs of cam-roller-spring mechanisms. In order to install the NSM, the length of the mass ring $l + b$ is longer than the rubber ring l. The shear modulus of the shaft and the rubber ring are G_0 and G_1, respectively. It should be noted that five cylindrical cams (3) are symmetrically distributed on a sleeve fixed on the shaft, and the rollers (4) are mounted on the slider (2) that is supported by a compressed linear spring (1). Certainly, the linear spring can be replaced by other structural elements, as long as it can provide elastic restoring force, such as elastomeric bearing or disk spring. Additionally, the rolling friction between the cam and the roller is insignificant and ignorable for the dispersion analysis, but it will be considered in numerical simulations to discuss its effect on wave attenuations.

At the static equilibrium position, no external torque is applied on the shaft, and all the centers of the cams, rollers and shaft are aligned on the same line, as shown in figures 1(c) and (d). Note that, as a schematic diagram in figure 1(a), eight HSLDS resonators are attached on the shaft. In fact, the number of resonators could be adjusted to suit practical needs. In order to demonstrate the advantage of this meta-shaft in comparison with the traditional locally resonant shaft, some parameters of the local resonators and the shaft are chosen from Yu *et al* [35]. All the parameters of the meta-shaft are tabulated in table 1.

Schematic diagrams of static analysis are shown in figure 2. Figure 2(a) shows the static equilibrium position of the resonators, and at such a position, the linear coil spring has a maximum compression ϑ, which is highlighted in red. When a

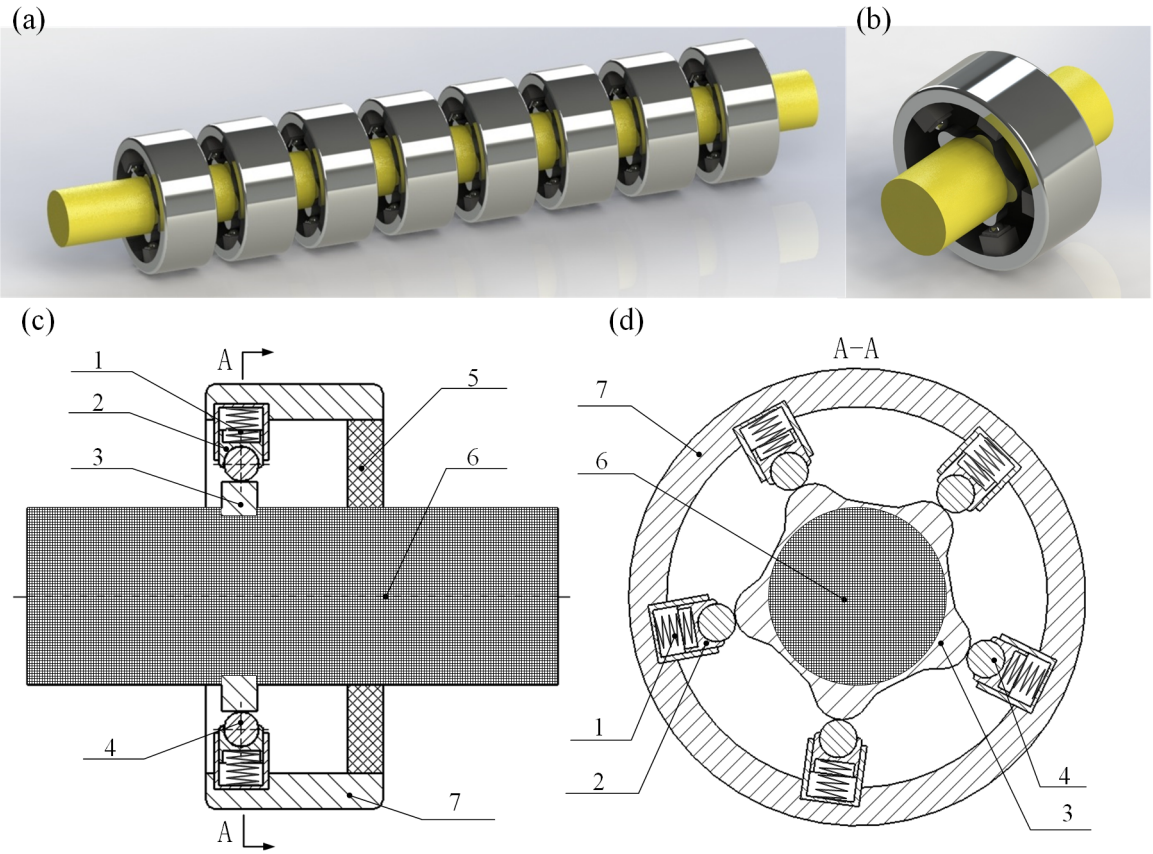

Figure 1. (a) Physical model of the meta-shaft, (b) physical model, (c) longitudinal-section view and (d) cross-section view of the HSLDS resonator.

torsional excitation acts on the meta-shaft, the shaft will vibrate and drive the resonators to turn around the shaft through the vulcanized rubber, which is depicted in figure 2(b). The coil springs in figure 2(b) are highlighted in orange, and the compression of this spring is relaxed when the roller deviates from the original position. With the increase of rotational angle, the compression of the coil spring is decreased. Consider only small-amplitude torsional oscillations and assume that the rollers and the cams always remain in contact. According to the geometrical relationship of the resonator, the static equilibrium equation of the HSLDS resonator can be given by

$$M = M_1 - 5Fd \tag{1}$$

where $M_1 = k_\theta \theta$ is the restoring torque of the rubber, F is the force provided by the compressed spring, $d = \delta r_3 \sin\theta / (r_1 + r_2)$ is the moment arm of F, M is the loading torque and k_θ is the effective torsional stiffness of the rubber ring, which is given as [35]

$$k_\theta = \frac{4\pi G_1 l}{r_0^2 - r_3^2} r_0^2 r_3^2. \tag{2}$$

The force provided by the compressed linear spring can be given by

$$F = \frac{k_h \alpha (r_1 + r_2)}{\delta - r_3 \cos\theta} \tag{3}$$

Table 1. Parameters of the meta-shaft.

Parameters	Descriptions	Values
G_0	Shear modulus of shaft	1.59×10^9 Pa
G_1	Shear modulus of rubber ring	3.4×10^5 Pa
G_2	Shear modulus of mass ring	1.49×10^{10} Pa
ρ	Density of shaft	1180 kg m^{-3}
ρ_1	Density of rubber ring	1300 kg m^{-3}
ρ_2	Density of mass ring	11 600 kg m^{-3}
r_0	Outer radii of the rubber ring	13.5 mm
r_1	Radii of the roller	2 mm
r_2	Radii of the cam	3 mm
r_3	Radii of the shaft	10 mm
r_4	Outer radii of the metal mass ring	16 mm
b	The length of the mass ring except the thickness of the rubber ring	15 mm
l	The thickness of the rubber ring	25 mm
ϑ	Pre-compression of coil spring	7 mm

where k_h is the stiffness of the linear spring. α and δ are geometrical coefficients, which can be written as

$$\alpha = \vartheta - (r_1 + r_2 + r_3) + \delta \tag{4}$$

$$\delta = r_3 \cos\theta + \sqrt{(r_1 + r_2)^2 - r_3^2 \sin^2\theta}. \tag{5}$$

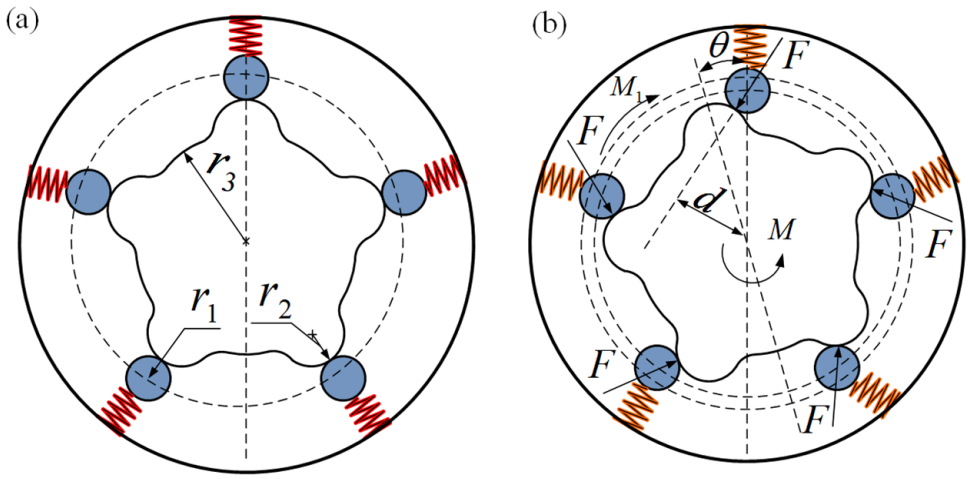

Figure 2. Schematic diagram of static analysis: (a) static equilibrium position; (b) position after additional torque acting on the shaft. The red color denotes the spring under maximum compression, and the orange color means that the compression of the spring is partly relaxed.

Substituting equation (3) into (1), the restoring torque of the HSLDS resonator can be calculated and given by

$$M = k_\theta \theta - 5\frac{k_h \alpha \delta r_3 \sin\theta}{\delta - r_3 \cos\theta}. \tag{6}$$

As mentioned before, the stiffness of the resonator can be reduced by adding a cam-roller-spring mechanism that provides negative stiffness. To design a resonator with desired low stiffness, a parameter β is introduced to denote the ratio of the net stiffness of the resonator to that of the rubber ring. Therefore, the restoring moment in equation (6) can be rewritten as

$$M = k_\theta \left[\beta\theta + (1-\beta)\,\theta - 5\varepsilon\frac{\alpha\delta r_3 \sin\theta}{\delta - r_3\cos\theta}\right] \tag{7}$$

where $\varepsilon = k_h/k_\theta$. The stiffness of the HSLDS resonator can be obtained by differentiating the restoring torque with respect to θ

$$k = k_\theta \left[\beta + (1-\beta) - 5\varepsilon\frac{p_1 - p_2}{(\delta - r_3\cos\theta)^2}\right] \tag{8}$$

where

$$p_1 = \left\{\frac{\mathrm{d}\delta}{\mathrm{d}\theta} r_3\delta\sin\theta + \alpha r_3\left(\delta\cos\theta + \frac{\mathrm{d}\delta}{\mathrm{d}\theta}\sin\theta\right)\right\}(\delta - r_3\cos\theta) \tag{9}$$

$$p_2 = \alpha r_3\delta\sin\theta\left(\frac{\mathrm{d}\delta}{\mathrm{d}\theta} + r_3\sin\theta\right). \tag{10}$$

In order to neutralize the stiffness by a ratio of $(1-\beta)$ and only keep a designated stiffness βk_θ at the static equilibrium position, one can let all the terms in equation (8) except βk_θ be zero,

$$(1-\beta) - 5\varepsilon\frac{p_1 - p_2}{(\delta - r_3\cos\theta)^2} = 0. \tag{11}$$

By substituting $\theta = 0$ into equation (11), a unique relationship for the parameters can be derived as

$$\varepsilon = \frac{(1-\beta)(r_1 + r_2)}{5\vartheta r_3 (r_1 + r_2 + r_3)} \tag{12}$$

By substituting equation (12) into (7) and (8), the net restoring torque and stiffness of the HSLDS resonator after a part of stiffness is counteracted by the NSM can be written as

$$M_{\mathrm{HSLDS}} = k_\theta\left[\theta - \frac{(1-\beta)(r_1 + r_2)}{\vartheta r_3 (r_1 + r_2 + r_3)}\frac{\alpha\delta r_3\sin\theta}{\delta - r_3\cos\theta}\right] \tag{13}$$

$$K_{\mathrm{HSLDS}} = k_\theta\left[1 - \frac{(1-\beta)(r_1 + r_2)}{\vartheta r_3 (r_1 + r_2 + r_3)}\frac{p_1 - p_2}{(\delta - r_3\cos\theta)^2}\right]. \tag{14}$$

The torsional stiffness of the resonator influenced by different geometrical parameters is plotted in figure 3 when the net stiffness ratio equals 0.5. As figure 3(a) shows, when the radii of the roller increases, the stiffness increases notably against the torsional angle, and strong nonlinearity appears. The effect of the radius of the cam on the stiffness is same as that of the radius of the roller, namely, with the increase of the radii, the stiffness plane becomes steeper and the nonlinearity becomes stronger. Figures 3(c) and (d) show the effects of the radius of the shaft and the pre-compression of the linear spring on the stiffness, respectively. Form figure 3(c), one can find that the shaft radii have slight influence on the stiffness. Compared with the effects of radii, the pre-compression of the linear spring has an opposite influence on the stiffness, namely, the stiffness plane becomes smooth and the nonlinear resonator grades into a linear one, with the increase of the pre-compression. Theoretically, a large compression, small radii of roller, cam and shaft are favorable to design a resonator with a wide displacement range of low stiffness. Combining the stiffness characteristic and mechanical design requirement, a set of parameters, $r_1 = 2, r_2 = 3, r_3 = 10, l = 7$, are selected for the following analysis.

The relationships of moment-angle and stiffness-angle for different net stiffness ratios are plotted in figure 4 according to equations (13) and (14) to indicate the effect of the NSM on the resonator. The red solid lines denote the moment and the torsional stiffness curves of the resonator, the black dotted lines indicate the moment and the stiffness provided by the cam-roller-spring mechanism and the blue dashed lines represent those provided by the rubber ring.

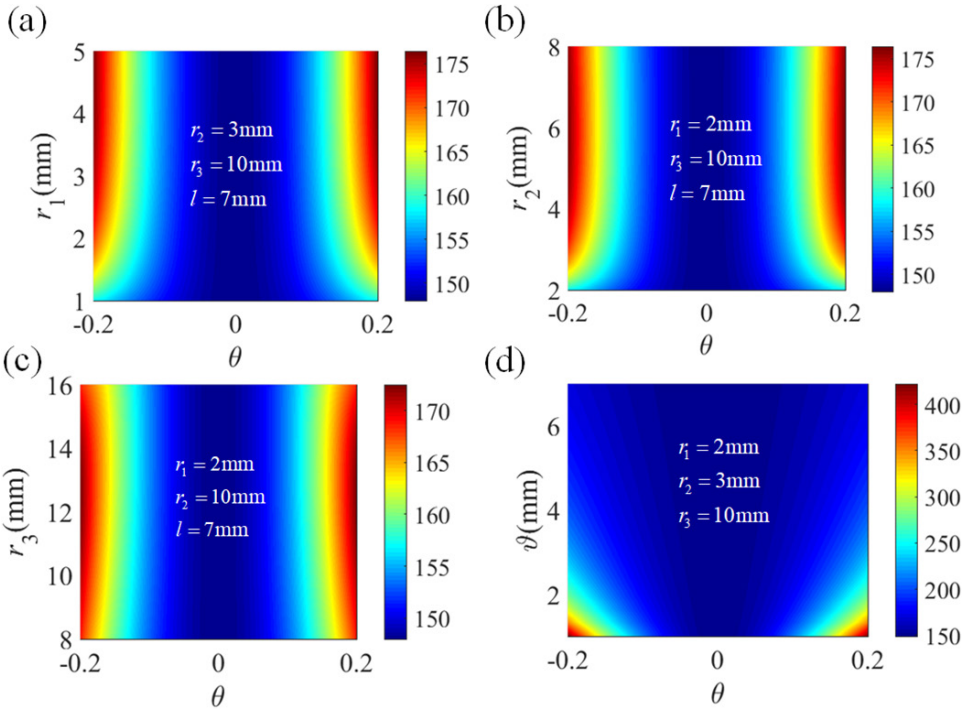

Figure 3. The torsional stiffness of the resonator influenced by the radii of the (a) roller, (b) cam, (c) shaft and (d) the pre-compression of the coil spring when the net stiffness equals 0.5 and the rubber ring remains unchanged.

As shown in figures 4(a) and (b), the blue dotted lines are covered by these red solid lines when the net stiffness ratio equals to 1, which means that the stiffness of the local resonator completely provided by the rubber ring, and the HSLDS resonator degenerates into a linear one. This linear resonator is identical to that presented by Yu *et al* [35], which is unable to realize a very low-frequency band gap. In this paper, the negative-stiffness mechanism is introduced into the linear resonator to substantially reduce its stiffness. As shown in figures 4(c) and (d), when the net stiffness ratio equals 0.5, as a special situation of figure 3, a half of the stiffness of the rubber ring is neutralized by the proposed NSM, and hence the net stiffness of the resonator is tuned towards half stiffness of the rubber ring at the static equilibrium position. In addition, the HSLDS resonator becomes a quasi-zero-stiffness one when the net stiffness ratio is as adjusted to become 0. In such a special case, the stiffness is zero at the static equilibrium position and close to zero in the vicinity of this position [44], as shown in figures 4(e) and (f). In addition, from these figures, it is clear that if the HSLDS resonator does not undergo a large-amplitude vibration, its nonlinear stiffness can be linearized as βk_θ at the static equilibrium position, which will be used in the following analysis for band structures.

3. Theoretical analysis

In this section, the linearized stiffness of the HSLDS resonator will be used to derive the analytical dispersion relations and obtain the band structures by using the transfer matrix method. In addition, the effects of the net stiffness ratio and the geometric parameters of the rubber ring on the band structures will also be discussed.

3.1. Dispersion relation

For a plain shaft without any resonators, the torsional vibration equations can be given by

$$\frac{\partial^2 \phi}{\partial t^2} = \frac{G_0 J_t}{\rho J_p} \frac{\partial^2 \phi}{\partial x^2} \tag{15}$$

where ϕ is the torsional displacement, G_0 the shear modulus, ρ the density of the shaft, J_t the torsional constant and J_p is the second polar moment of the cross-section, and $J_t = J_p = \pi r_3^4/2$. The harmonic responses of the shaft are assumed as $\phi(x,t) = \Phi(x) e^{i\omega t}$, where $\Phi(x)$ is the mode shape function, and the general solution for the mode shape function is

$$\Phi(x) = \Xi \sin(qx) + \Psi \cos(qx) \tag{16}$$

where Ξ and Ψ are the unknown parameters, $q = w/\sqrt{G_0/\rho}$ is the torsional wavenumber. For the ith unit cell, the mode shape function can be written as

$$\Phi_i(x_i) = \Xi_i \sin(qx_i) + \Psi_i \cos(qx_i) \tag{17}$$

where $x_i = x - il_c$ and $il_c \leqslant x \leqslant (i+1) l_c$ are local coordinates. l_c is the lattice constant, i.e. the length of the unit cell of the meta-shaft. The sketch of the meta-shaft with infinite length is shown in figure 5.

The equation of motion of the ith local resonator is given by

$$I \frac{\partial^2 \varphi_i(t)}{\partial t^2} + M(x_i, t) = 0 \tag{18}$$

where $I = \rho_2 \pi \left(r_4^2 - r_0^2\right)(l+b)\left(r_4^2 + r_0^2\right)/2$ is the moment of inertia of the nth HSLDS resonator, $M(x_i, t) =$

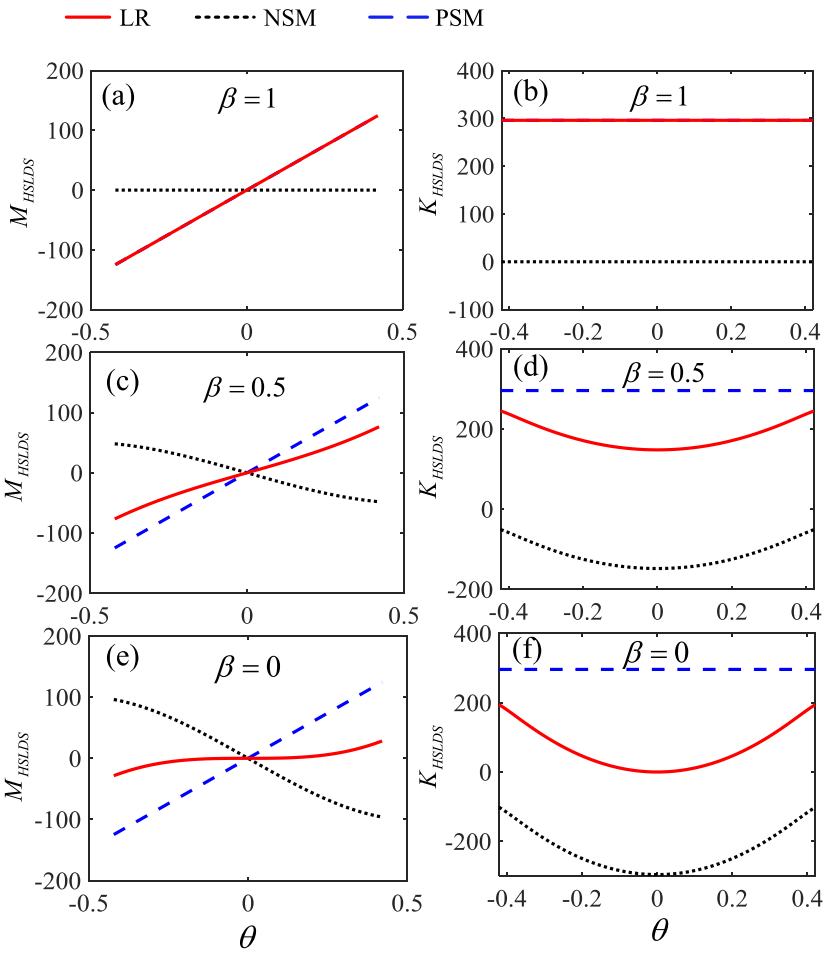

Figure 4. The moment and torsional stiffness of the resonator when the net stiffness ratio equals (a) and (b) $\beta = 1$; (c) and (d) $\beta = 0.5$; (e) and (f) $\beta = 0$. The red solid lines denote the moment and stiffness of the resonator, the black dotted lines the NSM and the blue dashed lines the rubber ring.

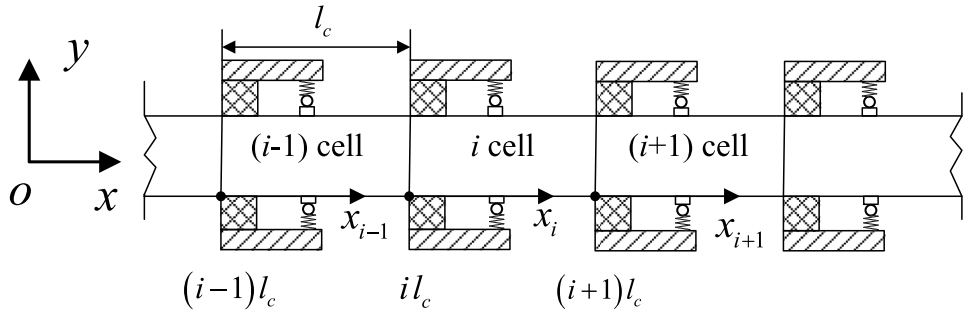

Figure 5. The sketch of the meta-shaft with an infinite length.

$\beta k_\theta [\varphi_i(t) - \phi_i(x_i, t)]$ is the internal torque between the resonator and the epoxy shaft and $\varphi_i(t)$ is the absolute angle of the ith resonator when an external excitation applied on the meta-shaft. The general solution for the ith resonator is assumed as $\varphi_i(t) = \Theta_i e^{i\omega t}$, where Θ_i is the amplitude of vibration. By substituting this general solution and equation (17) into (18), one can obtain the amplitude Θ_i

$$\Theta_i = \frac{\beta k_\theta \Phi_i(0)}{\beta k_n - I\omega^2}. \tag{19}$$

Therefore, the restoring torque $M(x_i, t)$ can be written as

$$M(x_i, t) = \frac{\beta k_\theta J_t \omega^2}{\beta k_\theta - J_t \omega^2} \Phi_i(0) e^{i\omega t}. \tag{20}$$

Considering the continuity of the torsional angle and the change of torque due to the connecting moment $M(x_i, t)$, one can obtain the following boundary conditions

$$\begin{cases} \Phi_{i-1}(l_c) = \Phi_i(0) \\ GJ_t \left[\frac{\partial \phi_{i-1}(x,t)}{\partial x}|_{x=l_c}\right] = GJ_t \left[\frac{\partial \phi_i(x,t)}{\partial x}|_{x=0}\right] + M(x_i, t) \end{cases}. \tag{21}$$

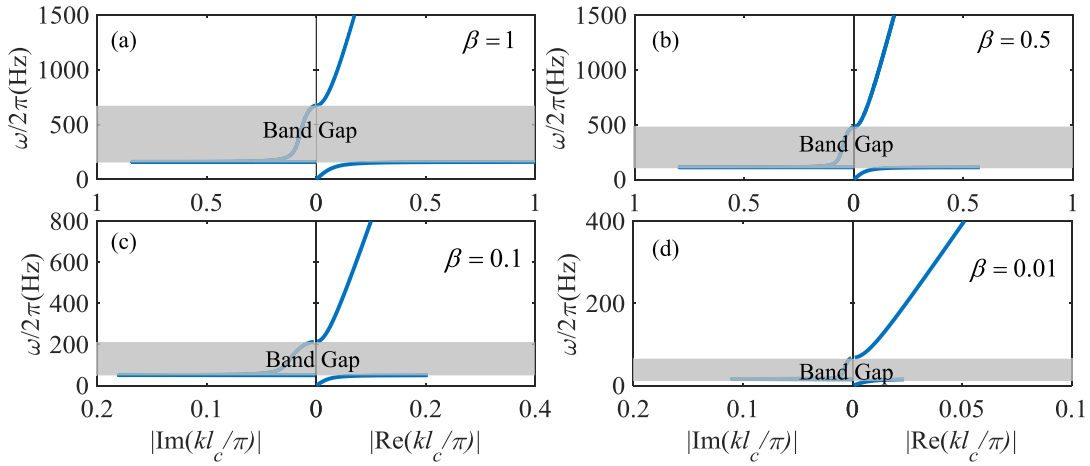

Figure 6. Theoretical band structures of the shaft with local resonator for different net stiffness when the residual stiffness ratio: (a) $\beta = 1$, (b) $\beta = 0.5$, (c) $\beta = 0.1$, (d) $\beta = 0.01$.

According to equation (21), one can obtain a matrix form expression for the unknown parameters of the $(i-1)$th and the ith resonators and can be written as

$$\mathbf{\Gamma}_i = \mathbf{\Delta}\mathbf{\Gamma}_{i-1} \tag{22}$$

where $\mathbf{\Gamma}_i = \{\Xi_i, \Psi_i\}^T$ and

$$\mathbf{\Delta} = \begin{pmatrix} -\frac{\omega^2\beta k_\theta I}{GJ_t q(\beta k_\theta - I\omega^2)}\sin(ql_c) + \cos(ql_c) & -\frac{\omega^2\beta k_\theta I}{GJ_t q(\beta k_\theta - I\omega^2)}\cos(ql_c) - \sin(ql_c) \\ \sin(ql_c) & \cos(ql_c) \end{pmatrix}. \tag{23}$$

For the meta-shaft, the vector Γ_i has to satisfy the Floquet–Bloch theorem,

$$\mathbf{\Gamma}_i = e^{ikl_c}\mathbf{\Gamma}_{i-1} \tag{24}$$

Remember that q is the wavenumber and l_c is the lattice constant. According to equation (22) and (24), one can obtain the dispersion relation of the meta-shaft

$$\left|\mathbf{\Delta} - e^{ikl_c}I\right| = 0 \tag{25}$$

where I is the unit matrix. For a given frequency, one can obtain a pair of complex values of the wave vector by solving the equation (25). If the imaginary part is zero, the frequency locates in the pass band. On the contrary, if the wave vector has non-zero imaginary part, the frequency belongs to the stopping band. Therefore, the band structure calculated by the transfer matrix method is a complex one, and the imaginary part can be utilized to delineate the torsional wave attenuation performance in the band gap.

3.2. Band structures

As shown in figure 6, the complex band structures are calculated for different net stiffness ratios. From these figures, it is clear that very low-frequency band gap can be opened by the proposed HSLDS resonator. With the net stiffness ratio decreasing (or the neutralized stiffness increasing), both the central frequency and the location of the band gap are shifted from a high frequency region to a low one. This can be attributed to the stiffness reduction by the NSM, which results in a very low resonant frequency of the HSLDS resonator.

Furthermore, the width and depth in figure 6 are represented by the non-zero imaginary part of the wavenumber. It can be observed that, with the decrease of the net stiffness ratio, the width of the band gap would become narrow, and the depth would get shallow, which implies that the performance of torsional wave attenuations become worse. However, in order to attenuate the torsional wave in a designated frequency region better, a broader and deeper band gap is expected. In this paper, several methods will be used to broaden the band gap and improve wave attenuations, such as increasing the number of unit cells and adjusting the parameter of the meta-shaft, which will be studied in detail in section 4.

3.3. Improvement regimes

In order to study improvement regimes of the torsional-wave band gap to broad the band width, the expressions of beginning and ending frequency are to be investigated firstly. As shown in figure 7(a), the mass ring resonates at this frequency $\omega_0 = \sqrt{I_1/k_\theta}$, which is the beginning frequency of the torsional wave band gap. When the shaft is not fixed, as shown in figure 7(b), the mass ring and the shaft resonate in opposite directions and the resonant frequency is $\omega_1 = \sqrt{k_\theta(I_1 + I_2)/I_1 I_2}$, which is the ending frequency of the band gap [45]. It is noteworthy that I_1, I_2 and k_θ denote the moment of inertia of the mass ring, the moment inertia of the shaft and the stiffness of the rubber ring highlighted in gray in figure 5, respectively.

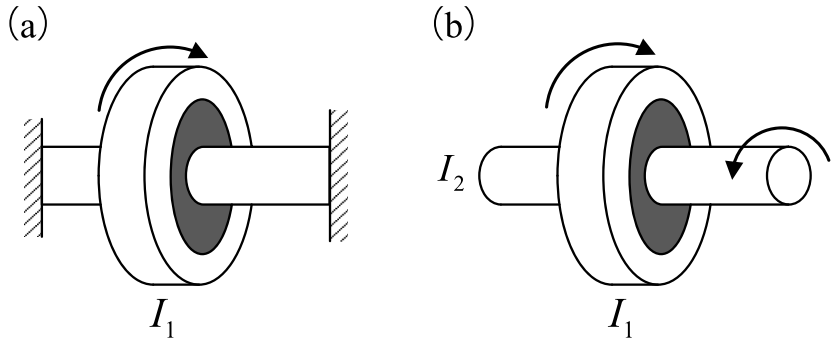

Figure 7. Analogous models corresponding to torsional vibration modes on the (a) beginning and (b) ending frequency of the LR band gap of the meta-shaft. The shading area denotes the rubber ring which provides torsional stiffness and support the mass ring.

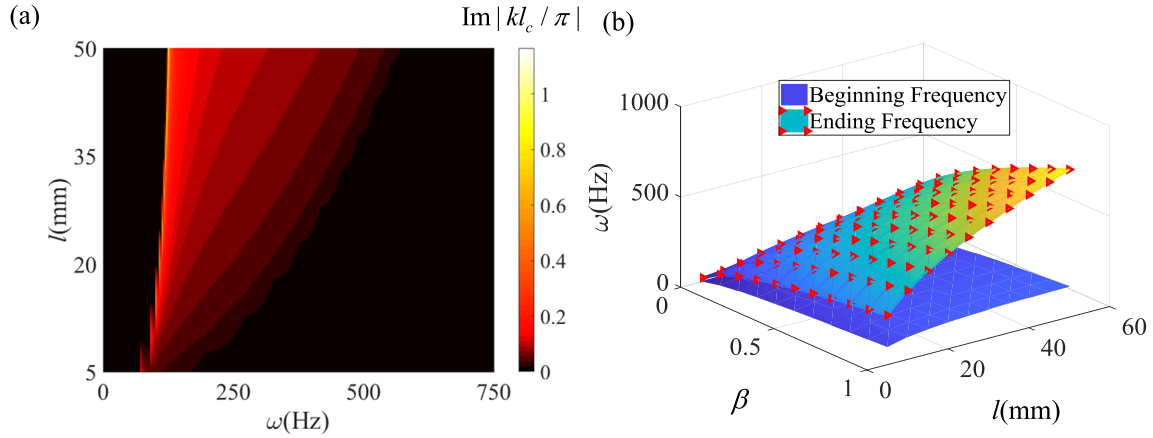

Figure 8. Influences of the net stiffness ratio and the thickness of rubber ring on band structures. (a) The imaginary part of the wave vector for different thickness of the rubber ring when the net stiffness ratio $\beta = 0.5$. (b) The beginning frequency and the ending frequency affected by both the net stiffness ratio and thickness of the rubber ring.

Substituting the expressions of the torsional stiffness of the rubber ring, the moments of inertia of the mass ring and the shaft into the expressions of beginning and the ending frequency, the edges of the torsional wave band gap can be given by

$$\omega_0 = \sqrt{\frac{\beta k_\theta}{I}} = \sqrt{\frac{8\beta l\pi G_1 r_0^2 r_3^2}{\rho_2\pi\left(r_0^2 - r_3^2\right)(l+b)\left(r_4^2 + r_0^2\right)\left(r_4^2 - r_0^2\right)}} \tag{26}$$

$$\omega_1 = \sqrt{\frac{8\beta\pi G_1 l r_0^2 r_3^2\left[\pi r_0^4 L\rho + \rho_2\pi\left(r_4^2 - r_0^2\right)\left(r_0^2 + r_4^2\right)(l+b)\right]}{\pi^2 r_3^4 L\rho\rho_2\left(r_4^2 - r_0^2\right)\left(r_0^2 + r_4^2\right)\left(r_0^2 - r_3^2\right)(l+b)}} \tag{27}$$

where L is the length of the meta-shaft. From equation (26) and (27), one can find that the thickness of the rubber ring is a key parameter for the band structure. The imaginary part of the wave vector is depicted as a function of the thickness l and the frequency in figure 8(a). The shining area denotes the band gap, where the imaginary part of the wave vector is non-zero. The brighter the color is, the better the performance of torsional wave attenuation is. Figure 8(b) shows a 3D plot of the beginning and ending frequencies of the band gap against both the net stiffness ratio and the thickness of the rubber ring, where one can observe the effects of these two parameters on the width of the band gap directly.

From figure 8, it is clear that, with the increase of the thickness of the rubber ring, the positive stiffness of the resonator increases, leading to enlargements in both the beginning and ending frequencies of the band gap. However, the increasing degree of the ending frequency is much larger than that of the beginning one. Therefore, the width of the band gap can be broadened by magnifying the thickness l. It also can be observed that, as the thickness increases, the color in the band gap becomes lighter, which implies the increase in the imaginary part of the wave vector. Hence, the performance of wave attenuation also can be improved by increasing the thickness of the rubber ring. Most importantly, the beginning frequency is impacted by the thickness l slightly, and thus the location of the band gap could stay in very low-frequency region, when a rubber ring with relatively large thickness is utilized to create a broad and deep band gap for attenuating torsional waves in a shaft. Furthermore, from figure 8(b), it can be seen that, with the decrease of the net stiffness, the location of the band gap moves from a high-frequency region to a low-frequency one, but the width would become narrow. Therefore, reasonable parameters of the resonator are essential to achieve an ideal band gap in the very low-frequency region.

4. Numerical results

To verify the band structure calculated by the transfer matrix method, and to demonstrate the wave attenuation, a meta-shaft with finite length under external random moment acting on the left-hand end of the shaft is studied by using the Galerkin method. The wave attenuation is evaluated by transmittance defined as a ratio of the torsion-angle amplitude at the right-hand end to that at the left-hand one. Both the effects of the number of unit cells and the exciting amplitude on the band structure will be discussed in this section.

4.1. The Galerkin method

For the finite-length meta-shaft under the random moment acting at the right-hand end ($x = 0$), the equation of motion can be yielded by using Newton's second law,

$$\rho J_p \frac{\partial^2 \phi}{\partial t^2} - G_0 J_t \frac{\partial^2 \phi}{\partial x^2} = M_R(t)\,\delta(x-0) + \sum_{m}^{n} M_{Re}(x_m,t)\delta(x-x_m) \tag{28}$$

where $M_R(t)$ is the random moment with a bandwidth from 1 to 1500 Hz. Remind that ρ is the density of the shaft, G_0 is the shear modulus of the shaft, J_p is the second polar moment of the cross-section with respect to the centroid and J_t is the torsional constant. Additionally, M_{Re} is the moment caused by the resonator, and acts at the attaching position of the resonator $x = x_m = ml_c$. By substituting the harmonic responses of the shaft $\phi(x_m,t)$ and the torsional angle of the mth local resonator $\varphi_m(t)$ into equation (13), M_{Re} can be given by

$$M_{Re}(x_m,t) = k_\theta \left\{\varphi_m(t) - \phi_m(x_m,t) - \frac{(1-\beta)(r_1+r_2)^2}{\vartheta r_3(r_1+r_2)(r_1+r_2+r_3)} \frac{\alpha\delta r_3 \sin[\varphi_m(t)-\phi_m(x_m,t)]}{\delta - r_3\cos[\varphi_m(t)-\phi_m(x_m,t)]}\right\}. \tag{29}$$

The harmonic responses of the meta-shaft are assumed to be

$$\phi(x_m,t) = \sum_{q=1}^{N} \Pi_q(x_m)\,\mu_q(t) \tag{30}$$

where N denotes the number of Galerkin truncation, $\Pi_q(x) = \cos(q\pi x/L)$ is the normal shape function of the shaft with free-free end condition, $\mu_q(t)$ denotes the generalized coordinate, and L is the total length of the shaft. In addition, the natural frequencies of the elastic shaft $\omega_q = q\pi c/L\,(q = 1, 2\cdots)$ are determined from the frequency equation $\sin(\omega l/c) = 0$, where $c = (G_0/\rho)^{1/2}$, and q is an integer and represents the order of eigenfunction. Note that the rigid-body displacement of the shaft is not considered in this paper. Substituting equation (30) into (28), the equation of motion of the meta-shaft can be rewritten as

$$\rho J_p \sum_{q=1}^{N} \Pi_q(x)\,\ddot{\mu}_q(t) - G_0 J_t \sum_{q=1}^{N} \Pi_q^{(2)}(x)\,\mu(t) = M_R(t)\,\delta(x-0) + \sum_{m}^{n} M_{Re}(x_m,t)\delta(x-x_m) \tag{31}$$

where the restoring torque is given by

$$M_{Re}(x_m,t) = k_\theta \left\{\varphi_m(t) - \sum_{q=1}^{N} \Pi_q(x_m)\,\mu_q(t) - \frac{(1-\beta)(r_1+r_2)}{\vartheta r_3(r_1+r_2+r_3)} \frac{\alpha\delta r_3 \sin\left[\varphi_m(t)-\sum_{q=1}^{N}\Pi_q(x_m)\mu_q(t)\right]}{\delta - r_3\cos\left[\varphi_m(t)-\sum_{q=1}^{N}\Pi_q(x_m)\mu_q(t)\right]}\right\}. \tag{32}$$

By introducing a weight function $\varphi_k(x)$, multiplying equation (31) by it and integrating the equation of motion from 0 to L, one can obtain

$$\rho J_p \sum_{q=1}^{N} \int_0^L \Pi_q(x)\,\varphi_k(x)\,\mathrm{d}x\ddot{\mu}_q(t) - G_0 J_t \sum_{q=1}^{N} \int_0^L \Pi_q^{(2)}(x)\,\varphi_k(x)\,\mathrm{d}x\mu(t) = \int_0^L \delta(x-0)\,\varphi_k(x)\,\mathrm{d}x M_R(t) + \sum_{m}^{n} \int_0^L \delta(x-x_m)\varphi_k(x)\,\mathrm{d}x M_{Re}(x_m,t), \quad k = 1,2,3,\cdots,N. \tag{33}$$

In order to decay the transient responses, both the modal damping of the shaft and the damping of the local resonator are taken into account in the numerical simulations. Note that it is difficult to identify the structural damping of the shaft and the damping in the resonator from rolling friction, so that the linear viscous damping are used to characterize the energy dissipation. Two parameters ζ_p and ζ_r are introduced to denote the damping ratio of the pth mode of the shaft and the local resonator, respectively. Due to the orthogonality of the mode function, equation (33) can be rewritten as a simplified form

$$I_p(q)\,\ddot{\mu}_q(t) + C_p(q)\,\dot{\mu}_q(t) + K_p(q)\,\mu_q(t) = \varphi_q(0)\,M_R(t) + \sum_{m}^{n} \varphi_q(x_m)\,M_{Re}(x_m,t) + \sum_{m}^{n} \varphi_q(x_m)\,M_{De}(x_m,t). \tag{34}$$

The derivation of equation (34) is given in appendix. For the resonator, the equation of motion can be written as

$$I\ddot{\varphi}_m + M_{Re}(x_m,t) + M_{De}(x_m,t) = 0 \tag{35}$$

where

$$I_p(q) = \frac{\rho J_p}{4}\left[2L + \frac{L\sin(2q\pi)}{q\pi}\right]; K_p(q) = \frac{G_0 J_t q\pi[2Lp\pi + L\sin(2q\pi)]}{4L^2};$$
$$C_p(q) = 2\zeta_p\sqrt{I_p K_p}; M_{De}(x_m,t) = 2\zeta_r\sqrt{Ik_\theta}\left[\dot{\varphi}_m(t) - \sum_{q=1}^{N}\Pi_q(x_m)\,\dot{\mu}_q(t)\right] \tag{36}$$

$M_{De}(x_m,t)$ denotes moment caused by the damping force of the local resonator, which acts at the attached position of the resonator.

4.2. Verification of the band gap

The material and geometrical parameters of the meta-shaft are listed in table 1, and the responses of the meta-shaft can be achieved by numerically solving the equations of motion, equations (34) and (35), by using the Runge–Kutta method. To make a comparison with the traditional resonator and highlight the advantage of the proposed resonator, a part of parameters of the meta-shaft is selected from the [35]. In this paper, the wave transmittance, defined as the ratio of the torsional angle at the right-hand end to that at the left-hand one, is used to evaluate the wave attenuation, which is presented in decibel (dB),

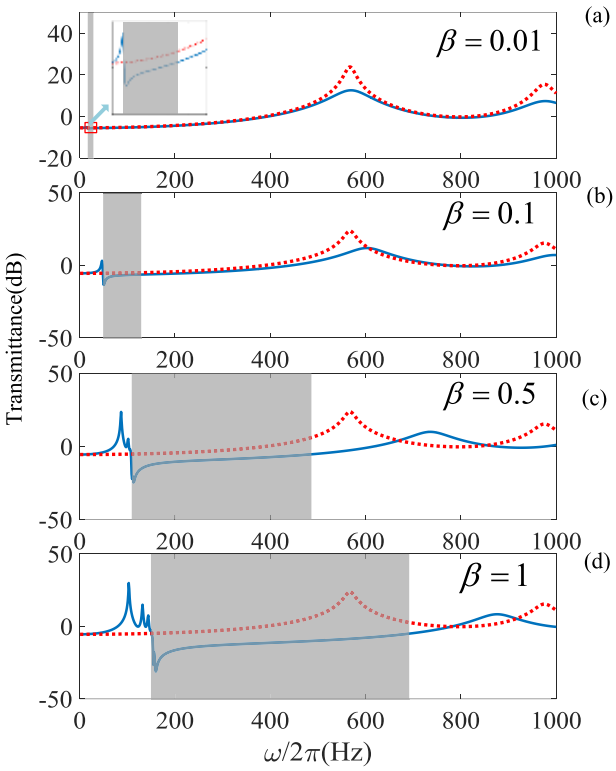

Figure 9. Wave transmittance calculated by numerical simulation by using Galerkin method when the net stiffness ratio is selected as: (a) $\beta = 0.01$, (b), $\beta = 0.1$, (c) $\beta = 0.5$, (d) $\beta = 1$. The shadow areas denote the band gap, and the number of unit cells is 20.

$$T = 20\log\left(\frac{\Theta_r}{\Theta_l}\right) \tag{37}$$

where Θ_r to Θ_l are the amplitudes of the responses of the torsional angle at the right-hand end ($x = N_{Re}l_c$) and left-hand end ($x = 0$), respectively, and N_{Re} is the number of the unit cells.

The minus wave transmittance in dB means torsional wave attenuation, and the corresponding frequency region denotes a band gap. Nevertheless, the positive wave transmittance in dB represents wave amplification, which implies the amplitude of the output signal at the right-hand end of the shaft is larger than that of the input signal at the left-hand end. It is true that $\Theta_r/\Theta_l < 1$ ($T < 0$) is expected to form a band gap.

However, in the very low-frequency region close to zero Hz, the minus wave transmittance does not imply wave attenuation, because the rigid-body mode is not considered in the numerical simulation. Nevertheless, the band structure is clear, even though the effect of the rigid-body mode on the structural responses might be obvious in very low-frequency region. With the increasing of the frequency, the contribution of the rigid-body mode becomes insignificant, and thus, both the band structure and the wave attenuation can achieve higher accuracies.

In figure 9, the dotted red lines denote the wave transmittance of the bare shaft (without resonators) and the solid blue lines represent the wave transmittance of the meta-shaft. From this figure, it is clear that this proposed shaft opens a very low-frequency band gap. As mentioned before, the central frequency of the band gap is dependent on the net stiffness ratio. Specifically, with the net stiffness decreasing, the central frequency moves from a high frequency to a low one. More importantly, by comparing figure 9 with 6, one can observe that the band structure calculated numerically by using the actually nonlinear stiffness matches well with the theoretical predication by using the linearized stiffness. Therefore, the linearized stiffness can be used to obtain the band structure when the meta-shaft does not suffer large-amplitude excitations. In addition, with the resonator stiffness decreasing, the performance of wave attenuation deteriorates, which also matches with the shallow band gap in figure 6.

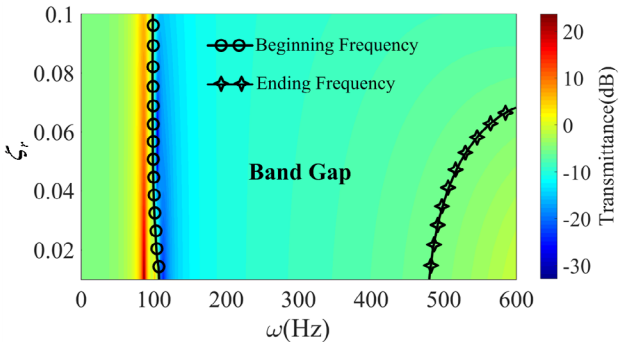

Figure 10. The damping of the local resonator on the wave transmittance.

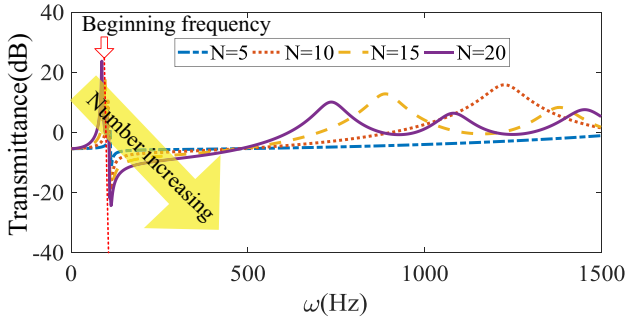

Figure 11. Influence of the number of unit cells on wave transmittance of the meta-shaft when $\beta = 0.5$, $\zeta_p = 0.02$ and $\zeta_r = 0.01$.

4.3. Influences of parameters

The influence of the damping of the local resonator on the wave transmittance is illustrated in figure 10. It is clear that, with the increasing of the damping ratio of the resonator, the performance of wave attenuation in the band gap gets worse, while the width of the band gap becomes broad. Particularly, the value of the wave transmittance is lower than zero in the high frequency region when the resonator has a relatively large damping.

Figure 11 shows the effect of the number of unit cells on the wave transmittance. In this figure, the wave transmittances of the meta-shaft with 5, 10, 15 and 20 unit cells are denoted by the blue solid line, red dotted line, saffron dashed line and purple dashed-dotted line, respectively. Obviously, with the

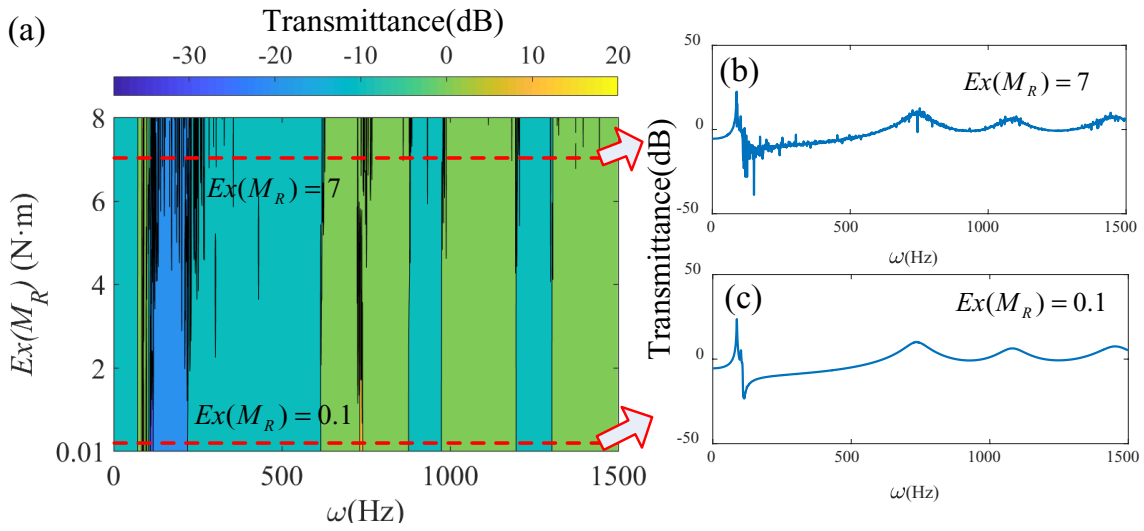

Figure 12. The wave transmittance influenced by the amplitude when the residual stiffness ratio equals 0.5, the number of unit cells equal 20 and the damping coefficient of the local resonator and the shaft equal 0.01 and 0.02, respectively.

increase of the number of unit cells, more peaks of the wave transmittance curve occur, and most importantly, the torsional wave attenuation in the band gap get better. Therefore, increasing the number of unit cells is a sound idea to attenuate the torsional wave as much as possible in the band gap.

As mentioned in section 2, the stiffness of the local resonator is nonlinear and can be influenced by the amplitude of the relative torsion angle between the resonator and the shaft. If the shaft undergoes a large-amplitude torsional vibration, the roller will deviate from the equilibrium position with a large angle and the local resonator will present a strong nonlinear stiffness. Therefore, a discussion about the effects of the exciting amplitude on the band gap and the wave attenuation performance is carried out.

Figure 12 shows the influence of the exciting amplitude on the wave transmittance. The contour map of the wave transmittances under different excitations is presented in figure 12(a). Also, the curves of wave transmittance for $Ex(M_R) = 7\,\mathrm{N}\cdot\mathrm{m}$ and $Ex(M_R) = 0.1\,\mathrm{N}\cdot\mathrm{m}$ are depicted in figures 12(b) and (c), respectively. Note that $Ex(M_R)$ denotes the expectation of the random exciting moment acting on the left-hand end of the meta-shaft.

From figure 12(a), it is clear that, as the exciting amplitude increases, the wave attenuation in the band gap would disappear at certain frequencies, such as 123 Hz, but be enhanced at some other frequencies, such as 151 Hz. This can be attributed to the fact that large-amplitude excitation would cause complicated dynamic behaviors, such as chaotic motions, which would result in new frequency components to counteract or amplify the responses at certain frequencies. In addition, in figure 12(a), there are some singular areas looking like black curves, which represent saltation (sudden change) of wave transmittance. The saltation also can be observed in figure 12(b), which is presented as spines on the transmittance curve. This phenomenon also can be attributed to the complicated dynamic responses caused by the nonlinear stiffness of the resonator under large excitations.

Moreover, by comparing figures 12(b) and (c), it can be observed that the wave transmittance curve under a small-amplitude excitation is smoother and the wave attenuation performance is better than those under a large-amplitude excitation. Therefore, this meta-shaft is excellent at attenuating torsional wave with small amplitude at low frequency. However, due to the amplitude-dependent feature of this meta-shaft, the large-amplitude wave might totally pass through the band gap, while the small-amplitude one is forbidden, which could be a potential application as an amplitude-dependent switch to control torsional waves.

5. Conclusions

In this paper, a torsional HSLDS local resonator is proposed for connecting a positive-stiffness element (a rubber ring) and a negative-stiffness mechanism (five pairs of cam-roller-spring mechanisms). The stiffness of the local resonator can be reduced substantially by the negative-stiffness mechanism. By attaching the proposed resonators on an epoxy shaft periodically, it becomes a meta-shaft. The dispersion relations are derived by using the transfer matrix method, which reveal that the central frequency of the band gap opened by the HSLDS resonator is much lower than that created by the linear resonator without the negative-stiffness mechanism.

The effects of system parameters on the band structure are also studied. With the thickness of the rubber ring increasing, the band width becomes broad and the wave attenuation performance is improved, which provides a potential solution to broaden and deepen the band gap in very low-frequency region. In addition, a large number of unit cells are also useful to obtain an ideal band gap with a large bandwidth and excellent wave attenuation. However, for a big excitation, the performance of wave attenuation would become worse, because the nonlinearity from the stiffness of the HSLDS resonator would be strong enough to cause complicated dynamic behaviour, when the resonator undergoes large-amplitude torsional

oscillations. Therefore, attaching a sufficient number of unit cells and avoiding large-amplitude excitations are suggested to achieve a broad and deep band gap for torsional wave attenuation in very-low-frequency region.

Acknowledgments

This research work was supported by National Key R&D Program of China (2017YFB1102801), National Natural Science Foundation of China (11572116), Natural Science Foundation of Hunan Province (2016JJ3036). The first author, Kai Wang, would like to thank the support from the China Scholarship Council (CSC).

Appendix

The following are the derivations for some equations appeared in this paper.

$$\begin{aligned}\rho I_p \sum_{q=1}^{N} \int_0^L \Pi_q(x)\,\varphi_k(x)\mathrm{d}x &= \rho I_p \sum_{q=1}^{N} \int_0^L \cos\left(\tfrac{q\pi x}{L}\right)\cos\left(\tfrac{k\pi x}{L}\right)\mathrm{d}x \\ &= \begin{cases} \rho I_p \sum_{p=1}^{N} \int_0^L \cos^2\left(\tfrac{q\pi x}{L}\right)\mathrm{d}x, & k=q; \\ 0 & \text{others.} \end{cases} \\ &= \begin{cases} \frac{\rho I_p}{4}\left[2L + \frac{L\sin(2q\pi)}{q\pi}\right], & k=q; \\ 0 & \text{others.} \end{cases}\end{aligned} \tag{A.1}$$

$$\begin{aligned}GI_t \sum_{q=1}^{N} \int_0^L \Pi_q^{(2)}(x)\,\varphi_k(x)\,\mathrm{d}x\mu(t) &= GI_t \sum_{q=1}^{N} \int_0^L \Pi_q^{(2)}(x)\,\varphi_k(x)\,\mathrm{d}x\mu(t) \\ &= -GI_t \sum_{q=1}^{N} \int_0^L \left(\tfrac{q\pi}{L}\right)^2 \cos\left(\tfrac{q\pi x}{L}\right)\cos\left(\tfrac{k\pi x}{L}\right)\mathrm{d}x\mu(t) \\ &= \begin{cases} -GI_t \sum_{q=1}^{N} \int_0^L \left(\tfrac{q\pi}{L}\right)^2 \cos\left(\tfrac{q\pi x}{L}\right)\cos\left(\tfrac{q\pi x}{L}\right)dx\mu(t), & q=k; \\ 0 & \text{others} \end{cases} \\ &= \begin{cases} -\frac{GI_t q\pi[2Lq\pi + L\sin(2q\pi)]}{4L^2}, & q=k; \\ 0 & \text{others} \end{cases}\end{aligned} \tag{A.2}$$

ORCID iDs

Jiaxi Zhou https://orcid.org/0000-0001-8348-6859
Huajiang Ouyang https://orcid.org/0000-0003-0312-0326

References

[1] Del Vescovo D and Giorgio I 2014 Dynamic problems for metamaterials: review of existing models and ideas for further research *Int. J. Eng. Sci.* **80** 153–72
[2] Khelif A, Choujaa A, Benchabane S, Djafari-Rouhani B and Laude V 2004 Guiding and bending of acoustic waves in highly confined phononic crystal waveguides *Appl. Phys. Lett.* **84** 4400–2
[3] Sun J H and Wu T T 2007 Propagation of acoustic waves in phononic-crystal plates and waveguides using a finite-difference time-domain method *Phys. Rev.* B **76** 104304
[4] Elnady T, Elsabbagh A, Akl W, Mohamady O, Garcia-Chocano V M, Torrent D, Cervera F and Sánchez-Dehesa J 2009 Quenching of acoustic bandgaps by flow noise *Appl. Phys. Lett.* **94** 2007–10
[5] Ho K M, Cheng C K, Yang Z, Zhang X X and Sheng P 2003 Broadband locally resonant sonic shields *Appl. Phys. Lett.* **83** 5566–8
[6] Wang T, Sheng M, Ding X and Yan X 2018 Wave propagation and power flow in an acoustic metamaterial plate with lateral local resonance attachment *J. Phys. D: Appl. Phys.* **51** 115306
[7] Yu D, Wen J, Zhao H, Liu Y and Wen X 2008 Vibration reduction by using the idea of phononic crystals in a pipe-conveying flui *J. Sound Vib.* **318** 193–205
[8] Li L X, Chen T N, Wang X P and Li B 2011 One-dimensional bi-stage phononic band gap shaft structure for reducing torsional vibration *Appl. Mech. Mater.* **141** 54–8
[9] Fleury R, Monticone F and Alù A 2015 Invisibility and cloaking: origins, present, and future perspectives *Phys. Rev. Appl.* **4** 1–20
[10] Zhu X, Liang B, Kan W, Zou X and Cheng J 2011 Acoustic cloaking by a superlens with single-negative materials *Phys. Rev. Lett.* **106** 014301
[11] He C, Ni X, Ge H, Sun X C, Chen Y Bin, Lu M H, Liu X P and Chen Y F 2016 Acoustic topological insulator and robust one-way sound transport *Nat. Phys.* **12** 1124–9
[12] Chen Z G and Wu Y 2016 Tunable topological phononic crystals *Phys. Rev. Appl.* **5** 054021
[13] Lv H, Tian X, Wang M Y and Li D 2013 Vibration energy harvesting using a phononic crystal with point defect states *Appl. Phys. Lett.* **102** 034103
[14] Hu G, Tang L and Das R 2018 Internally coupled metamaterial beam for simultaneous vibration suppression and low frequency energy harvesting *J. Appl. Phys.* **123** 055107
[15] Hussein M I, Leamy M J and Ruzzene M 2014 Dynamics of phononic materials and structures: historical origins, recent progress, and future outlook *Appl. Mech. Rev.* **66** 040802
[16] Jia Z, Chen Y, Yang H and Wang L 2018 Designing phononic crystals with wide and robust band gaps *Phys. Rev. Appl.* **9** 044021
[17] Lazarov B S and Jensen J S 2007 Low-frequency band gaps in chains with attached non-linear oscillators *Int. J. Non-Linear. Mech.* **42** 1186–93
[18] Xiao Y, Wen J and Wen X 2012 Broadband locally resonant beams containing multiple periodic arrays of attached resonators *Phys. Lett.* A **376** 1384–90
[19] Xiao Y, Wen J, Yu D and Wen X 2013 Flexural wave propagation in beams with periodically attached vibration absorbers: band-gap behavior and band formation mechanisms *J. Sound Vib.* **332** 867–93
[20] Xiao Y, Wen J, Huang L and Wen X 2014 Analysis and experimental realization of locally resonant phononic plates carrying a periodic array of beam-like resonators *J. Phys. D: Appl. Phys.* **47** 045307
[21] Wang X and Wang M Y 2016 An analysis of flexural wave band gaps of locally resonant beams with continuum beam resonators *Meccanica* **51** 171–8
[22] Wang T, Sheng M P and Qin Q H 2016 Multi-flexural band gaps in an Euler-Bernoulli beam with lateral local resonators *Phys. Lett.* A **380** 525–9
[23] Xiao Y, Wen J and Wen X 2012 Flexural wave band gaps in locally resonant thin plates with periodically attached springmass resonators *J. Phys. D: Appl. Phys.* **45** 195401

[24] Zhou X, Xu Y, Liu Y, Lv L, Peng F and Wang L 2018 Extending and lowering band gaps by multilayered locally resonant phononic crystals *Appl. Acoust.* **133** 97–106
[25] Bigoni D, Guenneau S, Movchan A B and Brun M 2013 Elastic metamaterials with inertial locally resonant structures: application to lensing and localization *Phys. Rev.* B **87** 174303
[26] Bacigalupo A and Gambarotta L 2017 Damped Bloch waves in lattices metamaterials with inertial resonators with inertial resonators *Procedia Eng.* **199** 1441–6
[27] Liu Z, Zhang X, Mao Y, Zhu Y Y, Yang Z, Chan C T and Sheng P 2000 Locally resonant sonic materials *Science* **289** 1734–6
[28] Frandsen N M M, Bilal O R, Jensen J S and Hussein M I 2016 Inertial amplification of continuous structures: large band gaps from small masses *J. Appl. Phys.* **119** 124902
[29] Li J and Li S 2018 Generating ultra wide low-frequency gap for transverse wave isolation via inertial amplification effects *Phys. Lett.* A **382** 241–7
[30] Liu C and Reina C 2018 Broadband locally resonant metamaterials with graded hierarchical architecture *J. Appl. Phys.* **123** 095108
[31] Wang M Y and Wang X 2013 Frequency band structure of locally resonant periodic flexural beams suspended with force–moment resonators *J. Phys. D: Appl. Phys.* **46** 255502
[32] Zhou J, Xu D and Bishop S 2015 A torsion quasi-zero stiffness vibration isolator *J. Sound Vib.* **338** 121–33
[33] Wang K, Zhou J and Xu D 2017 Sensitivity analysis of parametric errors on the performance of a torsion quasi-zero-stiffness vibration isolator *Int. J. Mech. Sci.* **134** 336–46
[34] Zheng Y, Zhang X, Luo Y, Zhang Y and Xie S 2018 Analytical study of a quasi-zero stiffness coupling using a torsion magnetic spring with negative stiffness *Mech. Syst. Signal Process.* **100** 135–51
[35] Yu D, Liu Y, Wang G, Cai L and Qiu J 2006 Low frequency torsional vibration gaps in the shaft with locally resonant structures *Phys. Lett.* A **348** 410–5
[36] Shu H, Zhao L, Shi X, Liu W and Li Z 2015 Torsional vibration band gaps in a shaft with 1D-piezoelectric phononic crystals *Noise Control Eng. J.* **63** 202–10
[37] Bishop R E D 1963 *Mechanical Vibrations* (Boston, MA: Allyn and Bacon)
[38] Hao Z and Cao Q 2015 The isolation characteristics of an archetypal dynamical model with stable-quasi-zero-stiffness *J. Sound Vib.* **340** 61–79
[39] Cao Q J, Wiercigroch M, Pavlovskaia E E, Grebogi C and Thompson J M T 2006 Archetypal oscillator for smooth and discontinuous dynamics *Phys. Rev.* E **74** 46215–8
[40] Liu C, Jing X and Li F 2015 Vibration isolation using a hybrid lever-type isolation system with an X-shape supporting structure *Int. J. Mech. Sci.* **98** 169–77
[41] Dong G, Zhang X, Xie S, Yan B and Luo Y 2017 Simulated and experimental studies on a high-static-low-dynamic stiffness isolator using magnetic negative stiffness spring *Mech. Syst. Signal Process.* **86** 188–203
[42] Zhou J, Wang K, Xu D and Ouyang H 2017 Local resonator with high-static-low-dynamic stiffness for lowering band gaps of flexural wave in beams *J. Appl. Phys.* **121** 044902
[43] Zhou J, Wang K, Xu D and Ouyang H 2017 Multi-low-frequency flexural wave attenuation in Euler–Bernoulli beams using local resonators containing negative-stiffness mechanisms *Phys. Lett.* A **381** 3141–8
[44] Carrella A, Brennan M J and Waters T P 2007 Static analysis of a passive vibration isolator with quasi-zero-stiffness characteristic *J. Sound Vib.* **301** 678–89
[45] Wang G, Shao L-H, Liu Y-Z and Wen J-H 2006 Accurate evaluation of lowest band gaps in ternary locally resonant phononic crystals *Chin. Phys.* **15** 1843–8